

**Key Points:**

- A triple mode of thermocline salinity (TMOS) variability was observed in the Pacific
- The TMOS is attributed to advection of anomalous salinity by the mean flow and advection of mean salinity by anomalous flow
- ENSO and PDO play an important role in generating TMOS

**Correspondence to:**

S. Hu,  
sjhu@qdio.ac.cn

**Citation:**

Hu, S., Sprintall, J., Guan, C., Hu, D., Wang, F., Lu, X., & Li, S. (2020). Observed triple mode of salinity variability in the thermocline of tropical Pacific Ocean. *Journal of Geophysical Research: Oceans*, 125, e2020JC016210. <https://doi.org/10.1029/2020JC016210>

Received 5 MAR 2020

Accepted 30 JUL 2020

Accepted article online 3 AUG 2020

## Observed Triple Mode of Salinity Variability in the Thermocline of Tropical Pacific Ocean

Shijian Hu<sup>1,2,3,4</sup> , Janet Sprintall<sup>5</sup> , Cong Guan<sup>1,2,3,4,6</sup> , Dunxin Hu<sup>1,2,3,4</sup>, Fan Wang<sup>1,2,3,4</sup> , Xi Lu<sup>1,2,4</sup>, and Shihan Li<sup>1,2,4</sup>

<sup>1</sup>CAS Key Laboratory of Ocean Circulation and Waves, Institute of Oceanology, Chinese Academy of Sciences, Qingdao, China, <sup>2</sup>Center for Ocean Mega-Science, Chinese Academy of Sciences, Qingdao, China, <sup>3</sup>Pilot National Laboratory for Marine Science and Technology (Qingdao), Qingdao, China, <sup>4</sup>College of Marine Science, University of Chinese Academy of Sciences, Qingdao, China, <sup>5</sup>Scripps Institution of Oceanography, University of California, San Diego, La Jolla, CA, USA, <sup>6</sup>Institute of Oceanographic Instrumentation, Shandong Academy of Sciences, Qingdao, China

**Abstract** A well-defined Triple MOde of Salinity (TMOS) variability in the tropical Pacific thermocline layer (24–25.5  $\sigma_0$  isopycnal surfaces) is revealed from the Argo observations during 2004–2018. Thermocline salinity in the tropical northern and southwestern Pacific Ocean varies out of phase on interannual to near-decadal time scales with that in the tropical southeastern Pacific Ocean. The TMOS is attributed to anomalous advection of mean salinity as well as advection of anomalous salinity by the mean oceanic current on isopycnal surfaces. While the TMOS pattern is quite different from the thermal patterns associated with the El Niño-Southern Oscillation (ENSO) or the Pacific Decadal Oscillation (PDO), it is significantly associated with the ENSO and PDO indices with a time lag of 10 months. Isopycnal propagation of salinity anomalies and anomalous freshwater input in the outcropping region, also both associated with ENSO and PDO, are important in the formation of TMOS. The propagation speed of isopycnal salinity anomalies is close to documented phase speeds of baroclinic Rossby waves and velocities of zonal currents. The TMOS acts to shape the basin-scale Pacific water masses and potentially plays an important role in climate.

**Plain Language Summary** Oceanic salinity changes from year-to-year influence water masses and the climate system. A 15-year time series of in situ salinity observations reveals a well-defined spatial pattern consisting of a Triple MODE of thermocline Salinity (TMOS) in the tropical Pacific Ocean. The TMOS is a result of anomalous advection of the mean thermocline salinity as well as the mean advection of anomalous salinity associated with the El Niño-Southern Oscillation (ENSO) and the Pacific Decadal Oscillation (PDO). Understanding the mechanisms responsible for setting up the TMOS pattern helps us to better understand how the climate may form and transform the Pacific water masses.

### 1. Introduction

Salinity variability plays an essential role in the ocean circulation and the climate system (Vinogradova et al., 2019). For example, the salinity effect is found to be important in understanding and predicting the El Niño-Southern Oscillation (ENSO) (e.g., Durack et al., 2012; Murtugudde & Busalacchi, 1998; Zhang et al., 2015; Zheng et al., 2015). Schneider (2000) proposed a decadal climate mode in the tropical Pacific Ocean, in which the salinity variability in the tropical central Pacific Ocean influences the surface heat budget that in turn affects the Pacific trade winds and the coupled ocean-atmosphere variability. The salinity response is also an important mechanism in controlling the interannual to decadal variability of the Indonesian Throughflow (Hu & Sprintall, 2016, 2017). On a longer time scale, the freshening salinity in the upper ocean caused by the intensified rainfall in the tropical oceans under a global warming scenario is thought to give rise to more intensified super typhoons (Balaguru et al., 2016).

Salinity in both the tropical North and South Pacific Ocean shows significant interannual to decadal variability. Sea surface salinity (SSS) variance at 2- to 5-year time scales has a maximum in the South Pacific Convergence Zone region, while at 5–10 years the maximum occurs in the subtropical regions in the Pacific Ocean (O’Kane et al., 2016). In the thermocline layer, isopycnal salinity anomalies are observed in the subtropics and off-equatorial tropics (10–14°N and 3–7°S) and advected to the central equatorial

©2020. The Authors.

This is an open access article under the terms of the Creative Commons Attribution-NonCommercial License, which permits use, distribution and reproduction in any medium, provided the original work is properly cited and is not used for commercial purposes.

Pacific Ocean by meridional flow (Li et al., 2012). Sustained freshening was observed during 2003–2011 and the subsurface salinity anomalies propagated southwestward in the northwest Pacific Ocean (Yan et al., 2013).

Different mechanisms are thought responsible for salinity variability depending on the depth range and time scales. SSS is largely controlled by surface freshwater flux, while mixed layer salinity is also affected by advection, mixing, entrainment, and nonlinear effects besides the sea surface freshwater flux (Hasson et al., 2013, 2014; Martins & Stammer, 2015). SSS variability on shorter time scales (from diurnal to intraseasonal) is primarily attributed to surface freshwater flux, but on longer (interannual to decadal) time scales, ocean dynamics are of greater importance (e.g., Köhl et al., 2014; Sprintall & Tomczak, 1992). The mechanisms that control salinity variability are also sensitive to regional dynamics. For example, the advection of freshwater is weak in the subpolar regions but of much more importance in the global tropical oceans (e.g., Ponte & Vinogradova, 2016).

Subduction and horizontal advection of salinity are thought to be important in the interannual to decadal fluctuation of ocean salinity in the thermocline layer salinity, which is typically on the isopycnal surfaces around  $\sigma_\theta = 24.5 \text{ kg m}^{-3}$  in the tropical Pacific Ocean (e.g., Gu & Philander, 1997; Katsura et al., 2013). The isopycnal  $\sigma_\theta = 24.5 \text{ kg m}^{-3}$  outcrops in the tropical northeastern and southeastern Pacific Ocean around  $\pm 20^\circ$  (e.g., Katsura et al., 2013). ENSO and the Pacific Decadal Oscillation (PDO) are found to influence the subduction and the interannual to decadal variability of thermocline salinity in the tropical Pacific Ocean (Du et al., 2015; Gu & Philander, 1997; Guan et al., 2019; Johnson et al., 2000; Lukas, 2001; Nurhati et al., 2011; Qu & Chen, 2009). Decadal fluctuation of the North Pacific Subtropical Mode Water was observed by the 137°E repeat hydrographic section (Oka et al., 2018) and suggested to be forced by winds over the central North Pacific (Oka et al., 2019). In the tropical South Pacific Ocean, the salinity variability on the  $24.5\sigma_\theta$  isopycnal has shown a dipole-like trend during 2004–2012 probably due to the decadal variability of evaporation minus precipitation (E–P) in the South Pacific Tropical Water mass formation region in the center of the South Pacific subtropical gyre (e.g., Zhang & Qu, 2014). In the equatorial Pacific Ocean, salinity is also influenced by Ekman upwelling due to the strong trade winds (Kao & Lagerloef, 2015; Lee et al., 2012; Sloyan et al., 2003).

Although previous studies have unmasked many important features as reviewed above, it is unclear yet in terms of any coherent spatial pattern of interannual to decadal variability of the basin-scale ocean salinity from a perspective of the whole tropical Pacific Ocean, which might differ from that in the South Pacific Ocean or North Pacific Ocean alone. A better understanding of the spatial pattern of salinity variability relies heavily on the accumulation of in situ salinity observations. The implementation of the Argo program has enabled a significant number of in situ salinity observations to be amassed since the early 2000s (Roemmich et al., 2009). The duration of the Argo era covers a complete PDO cycle and several ENSO cycles (Figure 1) and hence provides an opportunity to examine the basin-scale features of the interannual to near-decadal variability of thermocline salinity associated with these climate modes.

This paper explores the spatial mode of isopycnal salinity in the thermocline layer of the tropical Pacific Ocean using Argo observations and assimilations and investigates the physical processes forming the salinity mode associated with the ENSO and PDO. We describe data and methods in section 2 and present results in section 3, following by conclusions and discussion in section 4.

## 2. Data and Methods

We use the gridded Argo data set provided by Roemmich and Gilson (2009, RG Argo) to investigate the spatial pattern and temporal features of Pacific thermocline salinity variability. We examine the salinity on isopycnals between  $\sigma_\theta = 24 \text{ kg m}^{-3}$  and  $\sigma_\theta = 25.5 \text{ kg m}^{-3}$ , which constitutes a major component of the thermocline layer in the tropical Pacific Ocean (e.g., Katsura et al., 2013). The monthly RG Argo data set includes mapped temperature and salinity, using a weighted least squares fit to the Argo profiles over the period 2004–2018, and has a resolution of  $1^\circ \times 1^\circ$  horizontally and a vertical resolution of  $O(10 \text{ m})$  in the upper 170 db with coarser resolution below extending depths of 1,975 db. Figure 1 presents the amount of individual Argo float profiles (2004–2018) in the tropical Pacific Ocean and the variation of uncertainties in Argo salinity measurements (Wong et al., 2018).

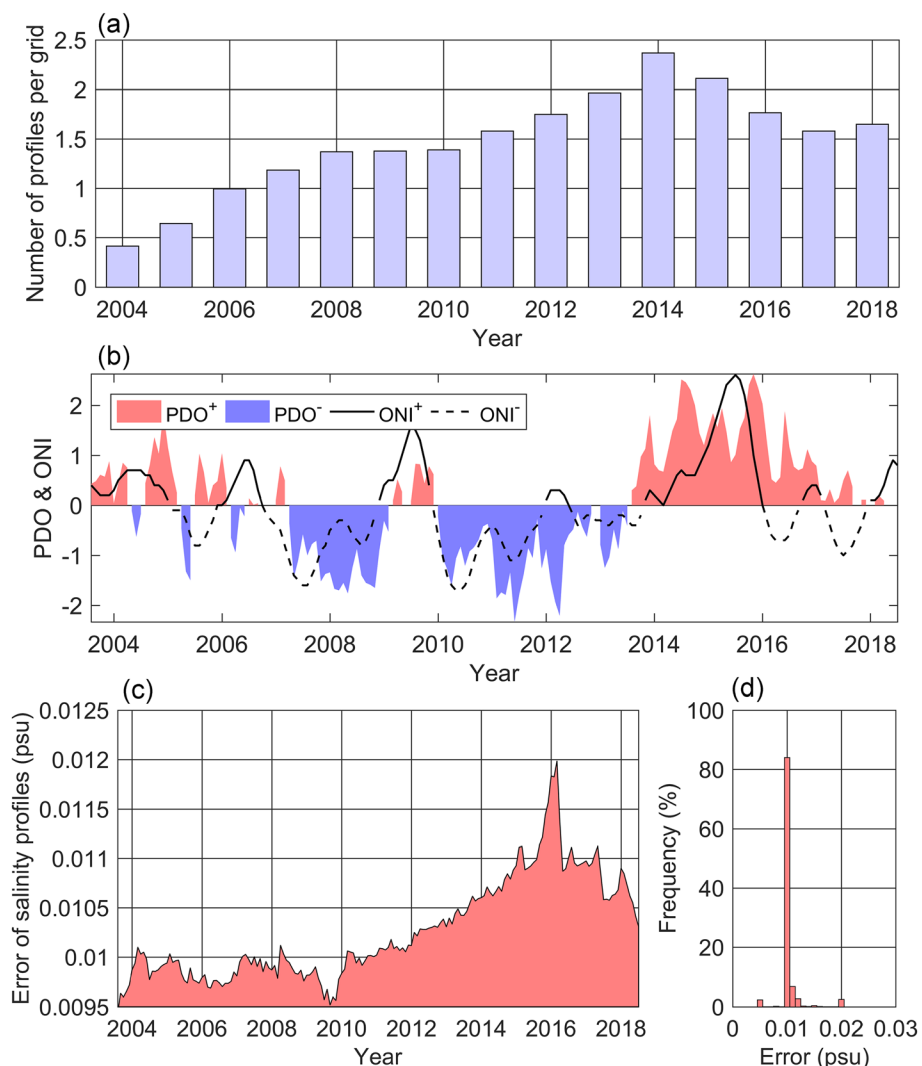


**Figure 1.** (a) Yearly number of Argo salinity profiles in each  $1^\circ \times 1^\circ$  grid box averaged over the tropical Pacific Ocean  $30^\circ\text{S}$  to  $30^\circ\text{N}$  and  $120^\circ\text{--}280^\circ\text{E}$ . PDO (positive PDO<sup>+</sup>) and ENSO indices (positive ONI<sup>+</sup>) are shown in the middle panel (b). Bottom panels present the mean error of salinity profiles in the tropical Pacific Ocean (c) and the frequency distribution of the errors in salinity profiles (d). See Wong et al. (2018) for detailed definition of errors in Argo salinity profiles.

The PDO index is computed using Extended Reconstruction of SSTs (Version 4) following the Mantua PDO index (Mantua et al., 1997). The Oceanic Niño Index (ONI) index is a time series of 3-month running mean of ERSST.v5 SST anomalies in the Niño 3.4 region ( $5^\circ\text{N}\text{--}5^\circ\text{S}$ ,  $120^\circ\text{--}170^\circ\text{W}$ ) and is provided by the Climate Prediction Center at the NOAA. The PDO index and ONI over the period 2004–2018 is shown in Figure 1b.

To examine the processes that control the variability of isopycnal salinity, a salinity budget is conducted using the Estimating the Circulation and Climate of the Ocean (ECCO) Version 4 Release 3 (ECCO v4.3), which assimilates observations into the Massachusetts Institute of Technology General Circulation Model forced by the ERA-Interim atmospheric reanalysis. ECCO has 50 vertical layers and a resolution of  $1^\circ$  longitude and  $1/3^\circ$  to  $1^\circ$  latitude and is available for the period between 1992 and 2015. The adjoint-based ECCO satisfies the equations of motion and conservation laws without artificial internal heat and freshwater sources/sinks (Wunsch & Heimbach, 2013). Previous studies show that the salinity pattern and variability are well reproduced by ECCO (e.g., Hu et al., 2019; Ponte & Vinogradova, 2016), and here it is used to examine the salinity budget terms and their respective roles in forming the triple mode of salinity (TMOS) pattern.

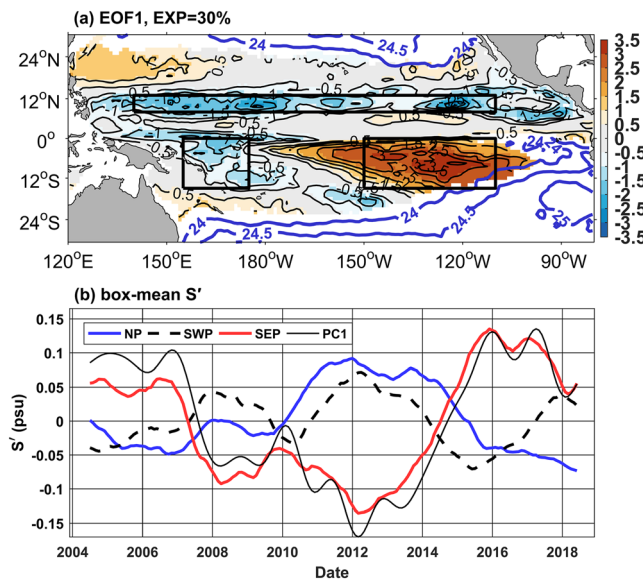


**Figure 2.** (a) The first EOF mode of the RG Argo salinity anomaly (black contours are every 0.01 psu) on isopycnal surface  $\sigma_\theta = 24.5 \text{ kg m}^{-3}$  (shaded area) and mean potential density  $24\text{--}25 \text{ kg m}^{-3}$  (thick blue lines) in December averaged over 2004–2018 at 20 db. (b) Comparison between normalized PC1 and box-mean salinity anomalies (psu) averaged over the northern Pacific box (NP,  $140\text{--}250^\circ\text{E}$ ,  $8\text{--}13^\circ\text{N}$ ), southwestern Pacific box (SWP,  $155\text{--}175^\circ\text{E}$ ,  $0\text{--}15^\circ\text{S}$ ), and southeastern Pacific box (SEP,  $210\text{--}250^\circ\text{E}$ ,  $0\text{--}15^\circ\text{S}$ ) shown in panel a. Blank area in panel a indicates missing data or outcropping of the isopycnal surface  $\sigma_\theta = 24.5 \text{ kg m}^{-3}$ .

The RG Argo potential temperature and salinity fields were mapped in  $z$  coordinate, and subsequently, the fields are interpolated into isopycnal coordinates. The isopycnal salinity ( $S$  [longitude, latitude,  $\sigma_\theta$ , time]) is low-passed with a 13-month cut-off Fourier filter. Empirical Orthogonal Functions (EOFs) of isopycnal salinity are formed at  $\sigma_\theta = 24, 24.5, 25$ , and  $25.5 \text{ kg m}^{-3}$  to investigate the spatial pattern of isopycnal salinity in the thermocline layer.

To the first order, the isopycnal salinity in the thermocline layer is controlled by

$$\frac{\partial S}{\partial t} = -\mathbf{u}\nabla S + Res, \quad (1)$$

where  $-\mathbf{u}\nabla S$  is the horizontal advection of salinity on the isopycnal surfaces and  $Res$  is the residual term including diapycnal advection and mixing processes (e.g., Feng et al., 1998). Isopycnal advection of salinity is calculated following

$$-\mathbf{u}\nabla S = -\left(u\frac{\partial S}{\partial x} + v\frac{\partial S}{\partial y}\right), \quad (2)$$

where the  $u$  and  $v$  are zonal and meridional current velocities on isopycnal surfaces and  $\frac{\partial S}{\partial x}$  and  $\frac{\partial S}{\partial y}$  are the zonal and meridional gradients of isopycnal salinity, respectively.

Assuming that  $\mathbf{u} = \bar{\mathbf{u}} + \mathbf{u}'$  and  $S = \bar{S} + S'$ , where overbar and prime, respectively, denote mean and anomaly. Changes in isopycnal salinity advection is hence

$$(-\mathbf{u}\nabla S)' = -\bar{\mathbf{u}}\nabla S' - \mathbf{u}'\nabla\bar{S} - \mathbf{u}'\nabla S', \quad (3)$$

where  $-\bar{\mathbf{u}}\nabla S'$  is the advection of anomalous salinity by the mean flow,  $-\mathbf{u}'\nabla\bar{S}$  is the advection of mean salinity by the anomalous flow, and  $-\mathbf{u}'\nabla S'$  is the advection of anomalous salinity by the anomalous current. The term  $-\mathbf{u}'\nabla S'$  is found to be very weak on an interannual to decadal time scale, and so, we do not include it in the discussion below.

### 3. Results

#### 3.1. Characteristics of the Spatial Mode of Thermocline Salinity Variability

The first two EOF modes of the monthly salinity on the isopycnal surface  $\sigma_\theta 24.5$  ( $S_{\sigma_\theta 24.5}$ ) explain about 30% and 12% of the total salinity variance, respectively. Figure 2a presents the spatial distribution of the first EOF mode (EOF1) of  $S_{\sigma_\theta 24.5}$ . The most pronounced feature of the spatial pattern of EOF1 is a clear triple mode of salinity (TMOS) in the thermocline layer, which includes two negative core regions in the northern tropical Pacific Ocean and southwestern tropical Pacific Ocean and a positive core region in the southeastern tropical Pacific Ocean during the positive phase of the first Principal Component (PC1). The spatial-mean monthly  $S_{\sigma_\theta 24.5}$  anomaly in the three regions (NP:  $140\text{--}250^\circ\text{E}$ ,  $8\text{--}13^\circ\text{N}$ ; SWP:  $155\text{--}175^\circ\text{E}$ ,  $15^\circ\text{S}\text{--}0^\circ$ ; SEP:  $210\text{--}250^\circ\text{E}$ ,  $15^\circ\text{S}\text{--}0^\circ$ ) are compared with the PC1 (Figure 2b). Interestingly, the  $S_{\sigma_\theta 24.5}$  anomaly in the SEP box ( $S'_{SEP}$ ) varies out of phase with that in the NP ( $S'_{NP}$ ) and SWP ( $S'_{SWP}$ ) boxes.

The correlation coefficient is  $-0.76$  between  $S'_{SEP}$  and  $S'_{NP}$ ,  $-0.75$  between  $S'_{SEP}$  and  $S'_{SWP}$ , and  $0.45$  between  $S'_{SWP}$  and  $S'_{NP}$ . All three correlation coefficients are statistically significant at 95% confidence level. The noteworthy covariance between the salinity variations in the three core regions implies that the salinity variability in the tropical Pacific Ocean as a whole constitutes an interlinked system and, therefore, the salinity fields in the three regions might be controlled by associated processes. The standard deviations (STDs) of  $S'_{NP}$ ,  $S'_{SEP}$ ,

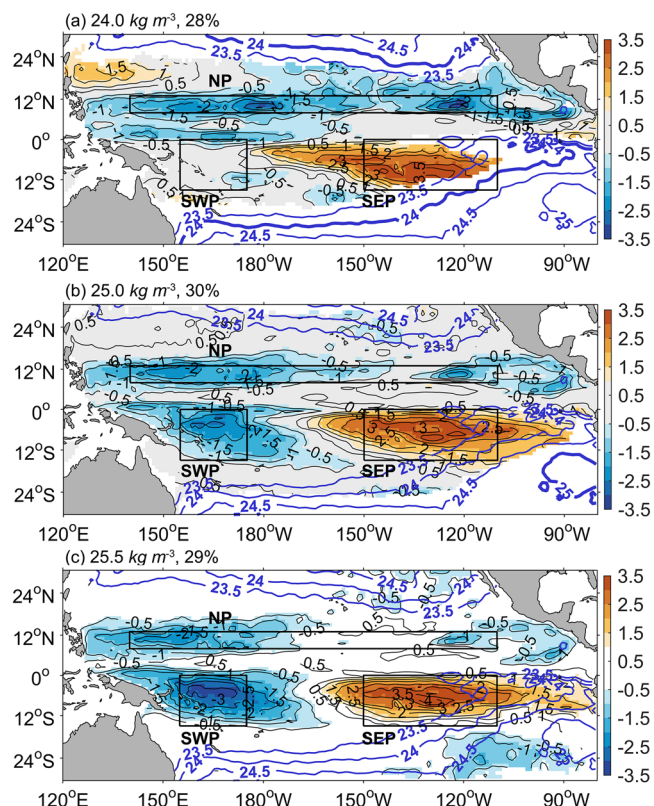


**Figure 3.** As in Figure 2a but for isopycnal surfaces (a) 24, (b) 25, and (c)  $25.5 \text{ kg m}^{-3}$ , where the TMOS explains 28%, 30%, and 29% of the total salinity variance, respectively. Thick blue lines indicate the mean potential density ( $23.5\text{--}25.5 \text{ kg m}^{-3}$ ) in December averaged over 2004–2018 at 20 db.

Both  $-\bar{\mathbf{u}}\nabla S'$  and  $-\mathbf{u}'\bar{\nabla S}$  are important to the anomalous advection term  $(-\mathbf{u}\nabla S')$ . Advection of mean salinity by anomalous current  $-\mathbf{u}'\bar{\nabla S}$  is negative in the southwestern and north Pacific Ocean and positive in the southeastern Pacific Ocean (Figure 4c). Advection of anomalous salinity by the mean flow  $(-\bar{\mathbf{u}}\nabla S')$  is positive in the southeastern Pacific Ocean but negative in the northern Pacific Ocean and has a similar magnitude with the TMOS (Figure 4d).

A comparison between the isopycnal salinity tendency  $(\frac{\partial S}{\partial t})$  and the anomalous advection term  $(-\mathbf{u}\nabla S')$  in the three boxes suggests that the anomalous advection of salinity explains most of the total salinity variability (Figures 4e–g). Correlation coefficients between  $\frac{\partial S}{\partial t}$  and  $(-\mathbf{u}\nabla S')$  are 0.9, 0.8, and 0.7 in the

SWP, SEP, and NP boxes, respectively. Although the correlation coefficients between  $\frac{\partial S}{\partial t}$  and  $(-\mathbf{u}\nabla S')$  in the SEP and NP boxes are relatively smaller than that in the SWP, probably due to the influence of vertical subduction in the outcropping regions in the SEP and NP boxes, the correlation coefficients between  $\frac{\partial S}{\partial t}$  and  $(-\mathbf{u}\nabla S')$  are statistically significant. STD of the anomalous advection of salinity in these boxes is close to the STD of the isopycnal salinity tendency  $(\frac{\partial S}{\partial t})$  in the corresponding boxes, and the STD of  $-\bar{\mathbf{u}}\nabla S'$  term is nearly equal to that of the  $-\mathbf{u}'\bar{\nabla S}$  term (Figure 4h), suggesting that the isopycnal advection of salinity explains a large portion of the salinity variability. Therefore, we conclude that the TMOS is attributed to anomalous advection of salinity on isopycnal surfaces due to both advection of mean salinity by anomalous oceanic current and advection of anomalous salinity by mean oceanic current.

and  $S'_{SWP}$  are 0.05, 0.08 and 0.04 psu, while the maximum amplitudes of salinity anomalies are 0.09, 0.14, and 0.07 psu, respectively. Hence, both STD and maximum amplitude in all three TMOS core regions are significantly greater than the error that is of  $O(0.01 \text{ psu})$  (Figure 1c). The EOF1 modes of monthly salinity on the isopycnal surface  $\sigma_\theta = 24, 25, 25.5 \text{ kg m}^{-3}$  ( $S_{\sigma_\theta 24}, S_{\sigma_\theta 25}, S_{\sigma_\theta 25.5}$ ) are also computed and show similar spatial patterns to that of the  $S_{\sigma_\theta 24.5}$  (Figure 3). We calculated the EOFs of temperature anomalies on the same density surfaces as well but did not find a corresponding pattern to TMOS (figures not shown).

### 3.2. Formation Mechanism of the TMOS

To investigate how the TMOS is formed, we employ ECCO assimilations. The EOF1 mode of ECCO salinity on isopycnal surface  $\sigma_\theta = 24.5 \text{ kg m}^{-3}$  (Figure 4a) is very similar to that determined from RG Argo (Figure 2a), indicating that the TMOS pattern is well presented by ECCO. The salinity advection terms  $((-\mathbf{u}\nabla S)', -\bar{\mathbf{u}}\nabla S', -\mathbf{u}'\bar{\nabla S})$  on isopycnal surface  $\sigma_\theta = 24.5 \text{ kg m}^{-3}$  were calculated using salinity, temperature, and horizontal velocity from the ECCO.

To examine the role of isopycnal advection of salinity in the formation of the TMOS, we compare the difference of isopycnal advection of salinity between positive TMOS phase ( $PC_1 > 0$ ) and negative TMOS phase ( $PC_1 < 0$ ) in Figures 4b–4d. The composited term of  $(-\mathbf{u}\nabla S)'$  shows a similar spatial pattern to the TMOS, which is positive in the southeastern tropical Pacific Ocean and negative in the tropical northern and southwestern Pacific Ocean (Figure 4b). The magnitude of the advection term  $(-\mathbf{u}\nabla S)'$  is close to the TMOS amplitude.

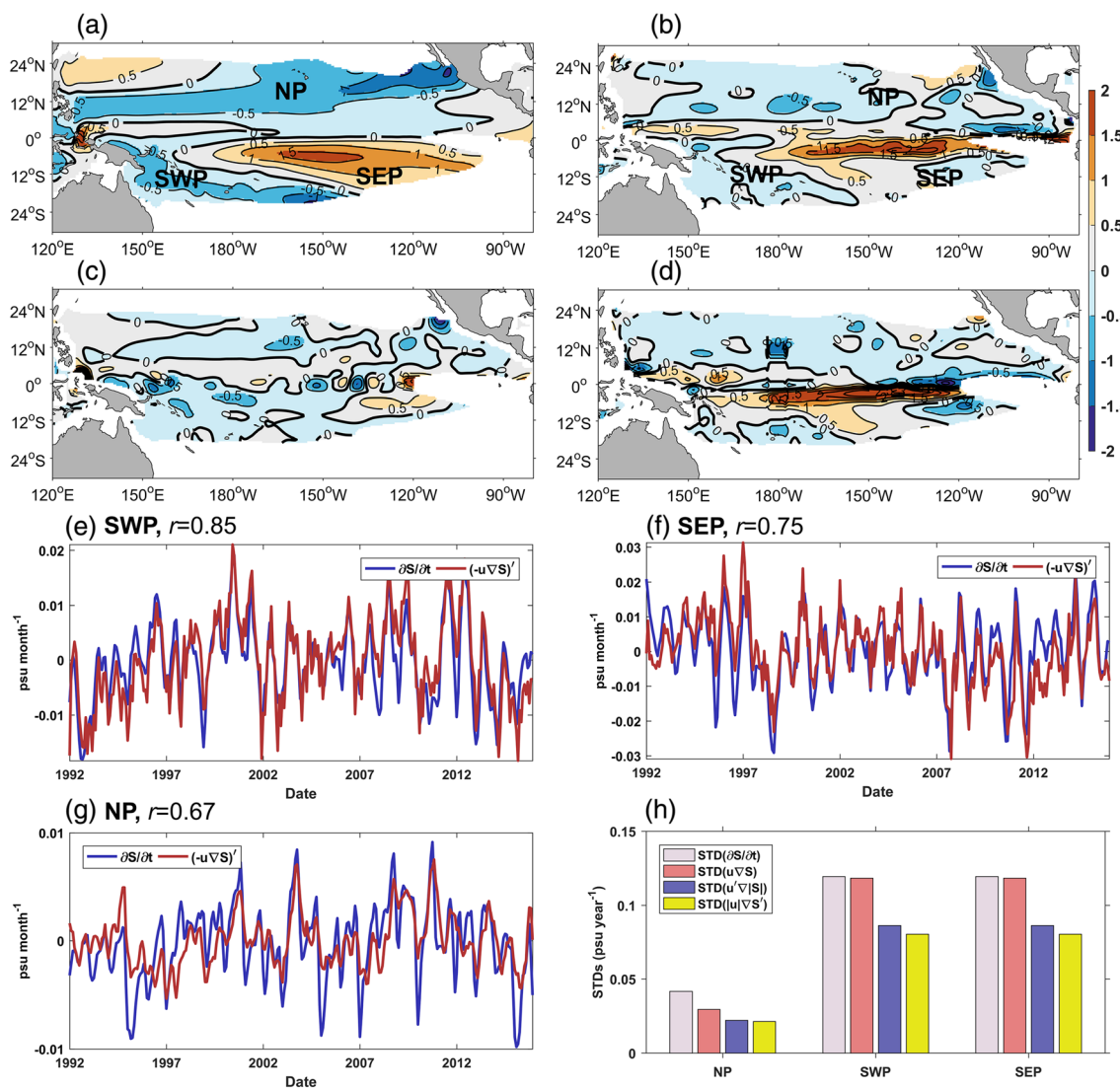


**Figure 4.** (a) The first EOF mode of the ECCO salinity anomaly (unit is 0.01 psu) on isopycnal surface  $\sigma_\theta = 24.5 \text{ kg m}^{-3}$  (shaded area). Panels b to d present composited differences (positive phase when  $\text{PC1} > 0$  minus that over negative phase when  $\text{PC1} < 0$ ) of (b) horizontal advection of salinity  $(-\bar{u} \frac{\partial S}{\partial x} - \bar{v} \frac{\partial S}{\partial y})$ , unit is 0.01 psu month $^{-1}$ , (c) horizontal advection of mean salinity by anomalous current  $(-\bar{u}' \frac{\partial \bar{S}}{\partial x} - \bar{v}' \frac{\partial \bar{S}}{\partial y})$ , unit in 0.01 psu month $^{-1}$ ) and (d) horizontal advection of anomalous salinity by mean current  $(-\bar{u}' \frac{\partial S'}{\partial x} - \bar{v}' \frac{\partial S'}{\partial y})$ , unit in 0.01 psu month $^{-1}$ ). Panels e to g show the comparison between isopycnal salinity change ( $\frac{\partial S}{\partial t}$ , psu month $^{-1}$ ) and anomalous horizontal advection term ( $(\bar{u} \nabla S)'$ , psu month $^{-1}$ ) averaged over the (e) SWP box, (f) SEP box, and (g) NP box. Variable  $r$  is the correlation coefficient between  $\frac{\partial S}{\partial t}$  and  $(\bar{u} \nabla S)'$ . Panel h is the STD of the isopycnal salinity tendency ( $\frac{\partial S}{\partial t}$ ) and anomalous salinity terms in the corresponding boxes.

### 3.3. Relationship to PDO and ENSO

ENSO and PDO are two major climate modes that describe the climate variability on interannual to decadal time scales. For example, Hu et al. (2020) found that the tropical Pacific Ocean circulation is significantly influenced by PDO. Hence, here we examine the relationship between the TMOS and ENSO/PDO. A comparison of the time series of TMOS (i.e., PC1) and the ENSO and PDO indices and their lead-lag correlation coefficients is shown in Figures 5a and 5b. The TMOS oscillates in phase with the PDO and ENSO cycle with a time lag: The PDO index leads the PC1 of TMOS by 10 months with a correlation coefficient of 0.9 that is significant above 99% confidence level, while the ENSO index leads the PC1 of TMOS by 10 months with a correlation coefficient of 0.6 that is also significant above 99% confidence level (Figure 5b).

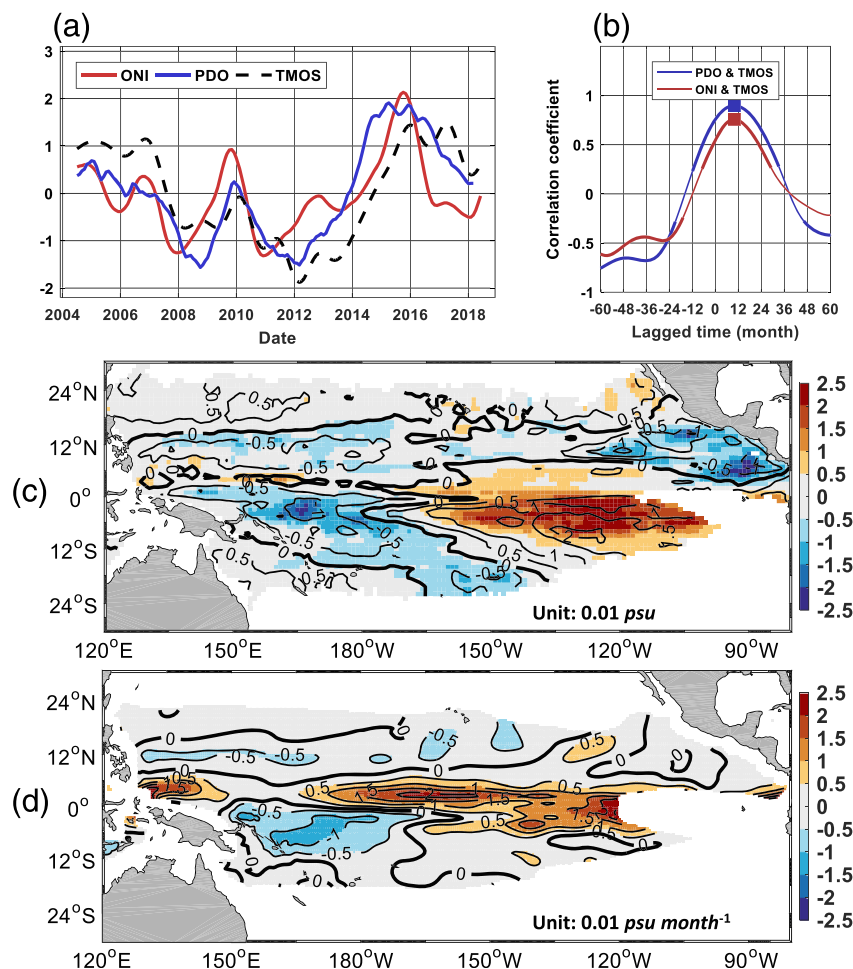


**Figure 5.** (a) Comparison of the time series of TMOS (i.e., the PC1 of EOF1) and the ONI and PDO indices. (b) Lead-lag correlation coefficients between the ONI and PDO indices and TMOS PC1 (positive lagged time indicates that the TMOS lags the climate indices and correlation coefficients that are significant at 99% confidence level are highlighted in heavy lines). Blue and red squares denote the maximum correlation coefficients. Panel c presents salinity anomalies at isopycnal surface ( $\sigma_0 = 24.5 \text{ kg m}^{-3}$ ) composed over positive phase minus negative phase of the PDO (black contour lines) and ONI (color shades) indices. Panel d shows the anomalous advection of salinity ( $0.01 \text{ psu month}^{-1}$ ) over positive PDO phases minus negative PDO phases.

The PDO index was in a negative phase over 2007–2014 with positive phases in 2004–2007 and 2015–2018. The ONI index shows clear positive peaks in 2005, 2009, and 2015 during three El Niño events and significant negative peaks in 2008, 2011, and 2018 during three La Niña events. During the positive phase of the PDO and during El Niño events, the Pacific salinity anomaly on isopycnal  $\sigma_0 = 24.5 \text{ kg m}^{-3}$  shows a triple pattern that is similar to the TMOS: positive in the southeastern Pacific and negative in the southwestern Pacific and northern tropical Pacific Ocean (Figure 5c). The comparison between the climate modes and the TMOS indicates that the PDO and ENSO cycles likely play an important role in forming and maintaining the Pacific TMOS.

Above, we showed that the TMOS pattern is attributed to the advection of salinity on isopycnal  $\sigma_0 = 24.5$ , so here we examine the difference of horizontal advection of salinity on the isopycnal surface  $\sigma_0 = 24.5$  between positive and negative phases of the ENSO and PDO (Figure 5d). The anomalous isopycnal advection of salinity during the positive ENSO/PDO phase relative to the negative phase explains the composited salinity anomaly during the positive phases and has a similar pattern with that composited over positive TMOS phases (Figure 5). Hence, ENSO and PDO may contribute to the TMOS through significant basin-scale anomalies of isopycnal advection of salinity.

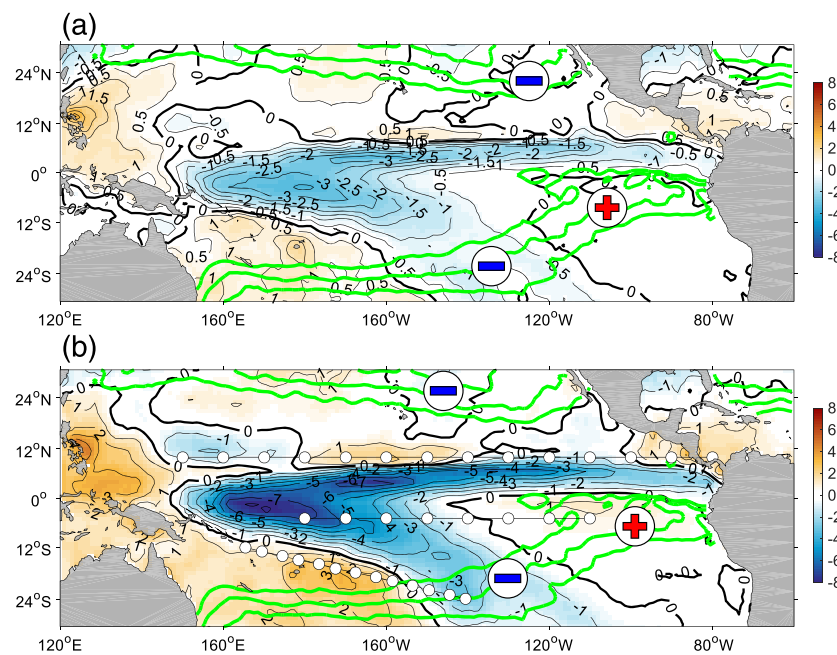


**Figure 6.** Composited E–P ( $\text{mm day}^{-1}$ ) averaged over positive phases of PDO (a) and ENSO (b) minus that of corresponding negative phases. Green contour lines indicate the isopycnal surfaces of  $\sigma_\theta = 23.5, 24$  and  $24.5 \text{ kg m}^{-3}$  at 20 db in December. Symbols “–” and “+” indicate negative and positive signs of E–P in the outcropping regions. Black lines inlaid with white dots denote the pathways mentioned in the following Figure 8.

### 3.4. Related Physical Processes

Two physical processes related to ENSO and PDO are expected to be important in the formation of the TMOS: anomalous surface freshwater input in the outcropping regions and horizontal propagation of salinity anomalies from the outcropping regions. In the tropical Pacific Ocean, the thermocline isopycnal outcrops in the eastern Pacific Ocean. Phase shifts of both ENSO and PDO are accompanied by significant changes in surface freshwater input in the outcropping regions. Figure 6 shows the composited difference of E–P over positive phases from negative phases. During the positive phases of ENSO and PDO, the outcropping region in the SEP has less surface freshwater input than negative phases, while the NP and SWP have more surface freshwater input (Figure 6).

Surface freshwater input freshens the sea surface and subsurface layer with a time lag due to subductions in the outcropping region. Figure 7 plots the lead-lag correlation coefficients between E–P and 5-db salinity anomaly and between 5-db and isopycnal surface  $\sigma_\theta = 24.5 \text{ kg m}^{-3}$ . It shows that salinity at 5 db is significantly related to E–P nearly simultaneously with a time lag close to zero in both the NEP ( $210\text{--}240^\circ\text{E}$ ,  $8\text{--}15^\circ\text{S}$ ) and SEP boxes (Figure 7a), while salinity on the isopycnal surface  $\sigma_\theta = 24.5 \text{ kg m}^{-3}$  is also significantly related to that at 5 db but with a time lag of about 6 to 8 months, which is associated with the subduction in the outcropping region.

The salinity signals associated with ENSO/PDO are propagated westward through anomalous advection of salinity caused by anomalous currents and/or anomalous salinity gradients, that is, anomalous advection of salinity. Here we present Hovmöller diagrams on isopycnal surface  $\sigma_\theta = 24.5 \text{ kg m}^{-3}$  along  $10^\circ\text{N}$ ,  $5^\circ\text{S}$  and along a pathway from the outcropping region in the South Pacific Ocean to the southwestern TMOS core region. Salinity anomalies that emerged in the outcropping regions are propagated westward and arrive at the western Pacific after a few months (Figure 8). The speeds of propagation of salinity anomalies are estimated by calculating the lead/lag time between two fixed points ( $160^\circ\text{E}$  and  $200^\circ\text{E}$  on the route of  $10^\circ\text{N}$ ;  $150^\circ\text{E}$  and  $200^\circ\text{E}$  on the route of  $5^\circ\text{S}$ ; and  $210^\circ\text{E}/22^\circ\text{S}$  and  $174^\circ\text{E}/14^\circ\text{S}$  on the southwest route) on the isopycnal surfaces shown in Figure 8. For example, for the NP box, we calculate the significant lead/lag time between salinity anomalies at  $160^\circ\text{E}/10^\circ\text{N}$  and  $200^\circ\text{E}/10^\circ\text{N}$  and the distance between

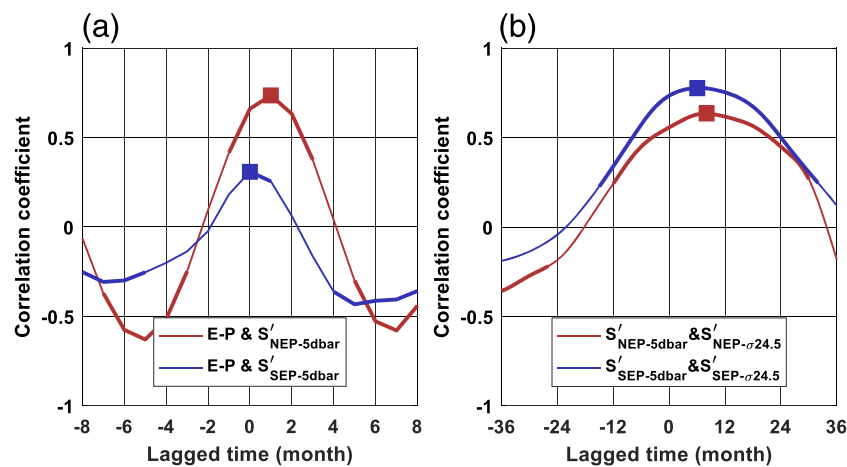


**Figure 7.** Lead-lag correlation coefficients between (a) E-P and salinity anomaly at 5 db, and (b) between 5-db and isopycnal surface  $\sigma_\theta = 24.5 \text{ kg m}^{-3}$  in NEP box (red, 210–240°E, 8–15°S) and SEP box (blue). Positive indicates E-P (a) or 5-db salinity leads. Correlation coefficients that are significant at 99% confidence level are highlighted in heavy lines. Squares denote peaks of correlation coefficients near zero lag.

the two points, and then roughly estimate the mean propagation speed, which is the distance divided by the time lag. We find that the propagation speeds of salinity anomalies are about  $0.17 \text{ m s}^{-1}$  in the NP box ( $10^\circ\text{N}$ ; Figure 8a),  $0.64 \text{ m s}^{-1}$  in the SEP box ( $5^\circ\text{S}$ ; Figure 8b), and  $0.32 \text{ m s}^{-1}$  along the SWP pathway (Figure 8c). The estimated propagation speeds are roughly close to mean speeds of zonal

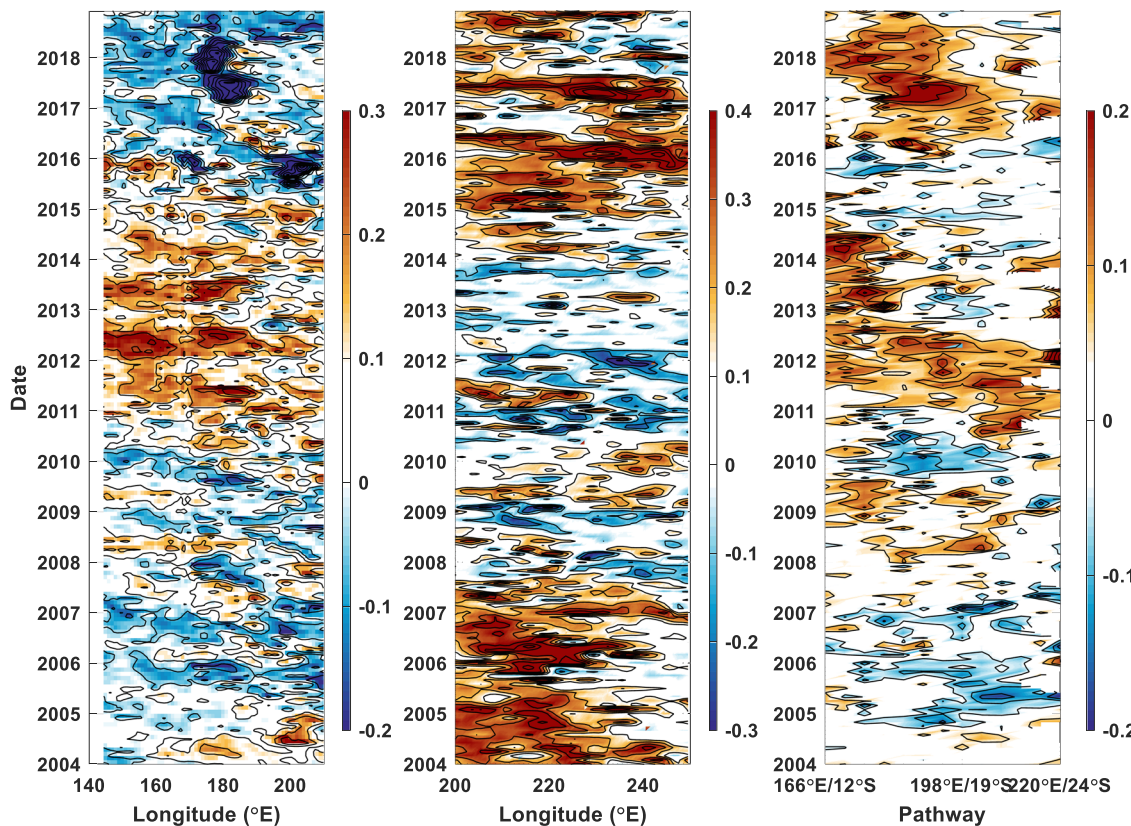


**Figure 8.** Hovmöller diagrams of salinity anomalies (psu) on isopycnal surface  $\sigma_\theta = 24.5 \text{ kg m}^{-3}$  along (a)  $10^\circ\text{N}$ , (b)  $5^\circ\text{S}$ , and (c) the pathway in the southwest Pacific Ocean shown in Figure 6.

currents at corresponding regions. For example, mean zonal velocity at 137°E/8°N is about westward 0.1 to 0.4 m s<sup>-1</sup> as shown in the multiyear shipboard acoustic Doppler current profiler measurements along 137°E (Hu & Hu, 2014, their Figure 3). In the SEP box, the ECCO assimilations indicate that zonal velocity at 240°E/5°S is about westward 0.30 m s<sup>-1</sup>, which is less than the speed of salinity propagation, which might be partly related to the ability of ECCO in reproducing the real ocean currents. Propagation of baroclinic Rossby waves are expected to induce fluctuations in horizontal ocean currents and hence might play an important role in the advection of salinity as well. The estimated propagation speeds match the phase speeds of baroclinic Rossby waves at corresponding latitudes (e.g., Chelton & Schlax, 1996). Previous studies have also shown that baroclinic Rossby waves due to ENSO and the PDO-related anomalous wind forcing propagate from the eastern Pacific Ocean and take several months to arrive at the western Pacific Ocean (e.g., Hu et al., 2016).

The time needed for subduction plus the time for isopycnal propagation is close to a year and roughly explains the time lag between ENSO/PDO indices and the PC1 of TMOS. Therefore, the subduction of ENSO/PDO-related surface salinity anomalies in the outcropping region and westward propagation of salinity anomalies on isopycnal surfaces are likely the major processes that account for the formation of TMOS.

#### 4. Summary

In this study, we have investigated the interannual to decadal variability of thermocline salinity in the Pacific Ocean on isopycnals centered at  $\sigma_\theta = 24.5$  kg m<sup>-3</sup> using 15-year in situ observations from Argo. A well-defined triple mode of thermocline salinity (TMOS) variability has been revealed by the first EOF mode of isopycnal salinity, which indicates that the salinity variability in the southeastern tropical Pacific Ocean is out of phase with that in the northern and southwestern tropical Pacific Ocean. The TMOS mode lags the ENSO and PDO indices by 10 months.

The role of isopycnal salinity advection and surface freshwater flux in the formation of the TMOS were examined. We conclude that the TMOS is attributed to PDO and ENSO-related anomalous advection of salinity on isopycnal surfaces due to both advection of mean salinity by anomalous oceanic current and also advection of the anomalous salinity by mean oceanic current. Anomalous oceanic currents in the thermocline layer and the anomalous sea surface freshwater input in the outcropping region in response to both the PDO and the ENSO cycle can cause anomalous advection of salinity on isopycnal surfaces. Baroclinic Rossby waves give rise to changes in the thermocline currents and lead to the anomalous advection of salinity on the time scale of months to years. Evidence shows that the ENSO/PDO cycle leads to changes in the surface freshwater input and salinity in the outcropping regions of the eastern Pacific Ocean and salinity anomalies then propagated from the outcropping regions to the west on the isopycnal surfaces in the thermocline layer.

It should be noted that surface heat flux variation in the eastern Pacific Ocean is likely important as well in driving the TMOS pattern. Using outputs from an ocean general circulation model, Ogata and Nonaka (2020) investigated the mechanisms of the decadal variability and recent trend of salinity observed along 137°E (Oka et al., 2017) and found that the surface heat flux variation in the eastern Pacific Ocean changes the meridional position of the outcropping region of  $25.4\sigma_\theta$  and hence exerts significant influence on the decadal variability of isopycnal salinity. Further studies are needed to explore the role of surface heat flux variability in the formation of TMOS.

The TMOS shapes the water mass structure of the tropical Pacific thermocline layer and hence is expected to exert influence on the stratification, ocean circulation, and climate system (e.g., Balaguru et al., 2016; Jyoti et al., 2019; Maes, 2008; Schneider, 2004). But to what extent the TMOS influences the ocean and climate system is as yet unknown. Hu et al. (2019) suggested that the PDO and ENSO signals give rise to significant interannual to decadal variability of thermocline salinity in the tropical Indian Ocean being transferred by the Indonesian Throughflow. Their results and the present work together suggest that the TMOS may act as the upstream part of the PDO/ENSO-controlled basin-scale water mass redistribution in the Indian and Pacific Oceans, but further studies are needed to link the salinity variability in the two ocean basins under the same framework.

## Data Availability Statement

The RG Argo data set was available online (at [http://sio-argo.ucsd.edu/RG\\_Climatology.html](http://sio-argo.ucsd.edu/RG_Climatology.html)). Argo profiles were distributed by the Ifremer (Institut français de recherche pour l'exploitation de la mer; at <ftp://ftp.ifremer.fr/ifremer/argo>). The Argo data were collected and made freely available by the International Argo Program and the national programs that contribute to it (<http://www.argo.ucsd.edu>, <http://argo.jcom-mops.org>). The Argo Program is part of the Global Ocean Observing System. The PDO index is available online (at <https://www.ncdc.noaa.gov/teleconnections/pdo>). The ONI index is provided by the U.S. National Oceanic and Atmospheric Administration, Climate Prediction Center (at [https://origin.cpc.ncep.noaa.gov/products/analysis\\_monitoring/ensostuff/ONI\\_v5.php](https://origin.cpc.ncep.noaa.gov/products/analysis_monitoring/ensostuff/ONI_v5.php)). The ECCO assimilations can be found at the NASA website (<https://ecco.jpl.nasa.gov/products/latest/>).

## Acknowledgments

This work benefits from the Northwestern Pacific Ocean Circulation and Climate Experiment (NPOCE)/CLIVAR program. S. H. was supported by the National Natural Science Foundation of China (Grants 41776018 and 91858101); the Strategic Priority Research Program of Chinese Academy of Sciences (CAS) (No. XDB42010403); the Key Research Program of Frontier Sciences, CAS (QYZDB-SSW-SYS023); the Key Deployment Project of Centre for Ocean Mega-Research of Science of CAS (Nos. COMS2019Q01 and COMS2019Q03); and the CAS-CSIRO Project Fund (No. 133244KYSB20190031). S. H. was a member of the Youth Innovation Promotion Association of CAS. J. S. was supported by the NOAA's Climate Program Office, Climate Variability and Predictability Program (Award Number NA17OAR4310257). C. G. and F. W. were supported by the National Natural Science Foundation of China (Grants 41806016 and 41730534). We are grateful to the two anonymous reviewers for their helpful comments.

## References

- Balaguru, K., Foltz, G. R., Leung, L. R., & Emanuel, K. A. (2016). Global warming-induced upper-ocean freshening and the intensification of super typhoons. *Nature Communications*, 7, 13670. <https://doi.org/10.1038/ncomms13670>
- Chelton, D. B., & Schlax, M. G. (1996). Global observations of oceanic Rossby waves. *Science*, 272(5259), 234–238. <https://doi.org/10.1126/science.272.5259.234>
- Du, Y., Zhang, Y., Feng, M., Wang, T., Zhang, N., & Wijffels, S. (2015). Decadal trends of the upper ocean salinity in the tropical Indo-Pacific since mid-1990s. *Scientific Reports*, 5, 16050. <https://doi.org/10.1038/srep16050>
- Durack, P. J., Wijffels, S. E., & Matear, R. J. (2012). Ocean salinities reveal strong global water cycle intensification during 1950 to 2000. *Science*, 336(6080), 455–458. <https://doi.org/10.1126/science.1212222>
- Feng, M., Hacker, P., & Lukas, R. (1998). Upper ocean heat and salt balances in response to a westerly wind burst in the western equatorial Pacific during TOGA COARE. *Journal of Geophysical Research*, 103(C5), 10,289–10,311. <https://doi.org/10.1029/97JC03286>
- Gu, D., & Philander, S. G. H. (1997). Interdecadal climate fluctuations that depend on exchanges between the tropics and extratropics. *Science*, 275(5301), 805–807. <https://doi.org/10.1126/science.275.5301.805>
- Guan, C., Hu, S., McPhaden, M. J., Wang, F., Gao, S., & Hou, Y. (2019). Dipole structure of mixed layer salinity in response to El Niño-La Niña asymmetry in the tropical Pacific. *Geophysical Research Letters*, 46, 12,165–12,172. <https://doi.org/10.1029/2019GL084817>
- Hasson, A., Delcroix, T., Boutin, J., Dussin, R., & Ballabreia-Poy, J. (2014). Analyzing the 2010–2011 La Niña signature in the tropical Pacific sea surface salinity using in situ data, SMOS observations, and a numerical simulation. *Journal of Geophysical Research: Oceans*, 119, 3855–3867. <https://doi.org/10.1002/2013JC009388>
- Hasson, A. E. A., Delcroix, T., & Dussin, R. (2013). An assessment of the mixed layer salinity budget in the tropical Pacific Ocean. *Observations and modelling (1990–2009)*. *Ocean Dynamics*, 63(2–3), 179–194. <https://doi.org/10.1007/s10236-013-0596-2>
- Hu, S., Hu, D., Guan, C., Wang, F., Zhang, L., Wang, F., & Wang, Q. (2016). Interannual variability of the Mindanao Current/Undercurrent in direct observations and numerical simulations. *Journal of Physical Oceanography*, 46(2), 483–499. <https://doi.org/10.1175/JPO-D-15-0092.1>
- Hu, S., & Sprintall, J. (2016). Interannual variability of the Indonesian Throughflow: The salinity effect. *Journal of Geophysical Research: Oceans*, 121, 2596–2615. <https://doi.org/10.1002/2015JC011495>
- Hu, S., & Sprintall, J. (2017). Observed strengthening of inter-basin exchange via the Indonesian seas due to rainfall intensification. *Geophysical Research Letters*, 44, 1448–1456. <https://doi.org/10.1002/2016GL072494>
- Hu, S., Sprintall, J., Guan, C., McPhaden, M. J., Wang, F., Hu, D., & Cai, W. (2020). Deep-reaching acceleration of global mean ocean circulation over the past two decades. *Science Advances*, 6, eaax7727. <https://doi.org/10.1126/sciadv.aax7727>
- Hu, S., Zhang, Y., Feng, M., Du, Y., Sprintall, J., Wang, F., et al. (2019). Interannual to decadal variability of upper ocean salinity in the southern Indian Ocean and the role of the Indonesian Throughflow. *Journal of Climate*, 32(19), 6403–6421. <https://doi.org/10.1175/JCLI-D-19-0056.1>
- Johnson, G. C., McPhaden, M. J., Rowe, G. D., & McTaggart, K. E. (2000). Upper equatorial Pacific Ocean current and salinity variability during the 1996–1998 El Niño-La Niña cycle. *Journal of Geophysical Research*, 105(C1), 1037–1053. <https://doi.org/10.1029/1999JC900280>
- Jyoti, J., Swapna, P., Krishnan, R., & Naidu, C. V. (2019). Pacific modulation of accelerated south Indian Ocean sea level rise during the early 21st century. *Climate Dynamics*, 53(7–8), 4413–4432. <https://doi.org/10.1007/s00382-019-04795-0>
- Kao, H.-Y., & Lagerloef, G. S. E. (2015). Salinity fronts in the tropical Pacific Ocean. *Journal of Geophysical Research: Oceans*, 120, 1096–1106. <https://doi.org/10.1002/2014JC010114>
- Katsura, S., Oka, E., Qiu, B., & Schneider, N. (2013). Formation and subduction of North Pacific tropical water and their interannual variability. *Journal of Physical Oceanography*, 43(11), 2400–2415. <https://doi.org/10.1175/JPO-D-13-031.1>
- Köhl, A., Martins, M. S., & Stammer, D. (2014). Impact of assimilating surface salinity from SMOS on ocean circulation estimates. *Journal of Geophysical Research: Oceans*, 119, 5449–5464. <https://doi.org/10.1002/2014JC010040>
- Lee, T., Lagerloef, G., Gierach, M. M., Kao, H.-Y., Yueh, S., & Dohan, K. (2012). Aquarius reveals salinity structure of tropical instability waves. *Geophysical Research Letters*, 39, L12610. <https://doi.org/10.1029/2012GL052232>
- Li, Y., Wang, F., & Sun, Y. (2012). Low-frequency spiciness variations in the tropical Pacific Ocean observed during 2003–2012. *Geophysical Research Letters*, 39, L23601. <https://doi.org/10.1029/2012GL053971>
- Lukas, R. (2001). Freshening of the upper thermocline in the North Pacific Subtropical Gyre associated with decadal changes of rainfall. *Geophysical Research Letters*, 28(18), 3485–3488. <https://doi.org/10.1029/2001GL013116>
- Maes, C. (2008). On the ocean salinity stratification observed at the eastern edge of the equatorial Pacific warm pool. *Journal of Geophysical Research*, 113, C03027. <https://doi.org/10.1029/2007JC004297>
- Mantua, N. J., Hare, S. R., Zhang, Y., Wallace, J. M., & Francis, R. C. (1997). A Pacific interdecadal climate oscillation with impacts on salmon production. *Bulletin of the American Meteorological Society*, 78(6), 1069–1079. [https://doi.org/10.1175/1520-0477\(1997\)078%3C1069:APICOW%3E2.0.CO;2](https://doi.org/10.1175/1520-0477(1997)078%3C1069:APICOW%3E2.0.CO;2)
- Martins, M. S., & Stammer, D. (2015). Pacific Ocean surface freshwater variability underneath the double ITCZ as seen by satellite sea surface salinity retrievals. *Journal of Geophysical Research: Oceans*, 120, 5870–5885. <https://doi.org/10.1002/2015JC010895>

- Murtugudde, R., & Busalacchi, A. J. (1998). Salinity effects in a tropical ocean model. *Journal of Geophysical Research*, 103(C2), 3283–3300. <https://doi.org/10.1029/97JC02438>
- Nurhati, I. S., Cobb, K. M., & Di Lorenzo, E. (2011). Decadal-scale SST and salinity variations in the central tropical Pacific: Signatures of natural and anthropogenic climate change. *Journal of Climate*, 24(13), 3294–3308. <https://doi.org/10.1175/2011JCLI3852.1>
- O'Kane, T. J., Monselesan, D. P., & Maes, C. (2016). On the stability and spatiotemporal variance distribution of salinity in the upper ocean. *Journal of Geophysical Research: Oceans*, 121, 4128–4148. <https://doi.org/10.1002/2015JC011523>
- Ogata, T., & Nonaka, M. (2020). Mechanisms of long-term variability and recent trend of salinity along 137°E. *Journal of Geophysical Research: Oceans*, 125, e2019JC015290. <https://doi.org/10.1029/2019jc015290>
- Oka, E., Ishii, M., Nakano, T., Suga, T., Kouketsu, S., Miyamoto, M., et al. (2018). Fifty years of the 137°E repeat hydrographic section in the western North Pacific Ocean. *Journal of Oceanography*, 74(2), 115–145. <https://doi.org/10.1007/s10872-017-0461-x>
- Oka, E., Katsura, S., Inoue, H., Kojima, A., Kitamoto, M., Nakano, T., & Suga, T. (2017). Long-term change and variation of salinity in the western North Pacific subtropical gyre revealed by 50-year long observations along 137°E. *Journal of Oceanography*, 73(4), 479–490. <https://doi.org/10.1007/s10872-017-0416-2>
- Oka, E., Yamada, K., Sasano, D., Enyo, K., Nakano, T., & Ishii, M. (2019). Remotely forced decadal physical and biogeochemical variability of North Pacific subtropical mode water over the last 40 years. *Geophysical Research Letters*, 46, 1555–1561. <https://doi.org/10.1029/2018gl081330>
- Ponte, R. M., & Vinogradova, N. T. (2016). An assessment of basic processes controlling mean surface salinity over the global ocean. *Geophysical Research Letters*, 43, 7052–7058. <https://doi.org/10.1002/2016GL069857>
- Qu, T., & Chen, J. (2009). A North Pacific decadal variability in subduction rate. *Geophysical Research Letters*, 36, L22602. <https://doi.org/10.1029/2009GL040914>
- Roemmich, D., & Gilson, J. (2009). The 2004–2008 mean and annual cycle of temperature, salinity, and steric height in the global ocean from the Argo Program. *Progress in Oceanography*, 82(2), 81–100. <https://doi.org/10.1016/j.pocean.2009.03.004>
- Roemmich, D., Johnson, G. C., Riser, S., Davis, R., Gilson, J., Owens, W. B., et al. (2009). The Argo Program: Observing the Global Ocean with profiling floats. *Oceanography*, 22(2), 34–43. <https://doi.org/10.5670/oceanog.2009.36>
- Schneider, N. (2000). A decadal spiciness mode in the tropics. *Geophysical Research Letters*, 27(2), 257–260. <https://doi.org/10.1029/1999GL002348>
- Schneider, N. (2004). The response of tropical climate to the equatorial emergence of spiciness anomalies. *Journal of Climate*, 17(5), 1083–1095. [https://doi.org/10.1175/1520-0442\(2004\)017<1083:TROTCT>2.0.CO;2](https://doi.org/10.1175/1520-0442(2004)017<1083:TROTCT>2.0.CO;2)
- Sloyan, B. M., Johnson, G. C., & Kessler, W. S. (2003). The Pacific cold tongue: A pathway for interhemispheric exchange. *Journal of Physical Oceanography*, 33(5), 1027–1043. [https://doi.org/10.1175/1520-0485\(2003\)033<1027:TPCTAP>2.0.CO;2](https://doi.org/10.1175/1520-0485(2003)033<1027:TPCTAP>2.0.CO;2)
- Sprintall, J., & Tomczak, M. (1992). Evidence of the barrier layer in the surface layer of the tropics. *Journal of Geophysical Research*, 97(C5), 7305–7316. <https://doi.org/10.1029/92JC00407>
- Vinogradova, N., Lee, T., Boutin, J., Drushka, K., Fournier, S., Sabia, R., et al. (2019). Satellite salinity observing system: Recent discoveries and the way forward. *Frontiers in Marine Science*, 6, 243. <https://doi.org/10.3389/fmars.2019.00243>
- Wong, A., Keeley, R., & Carval, T. (2018). Argo quality control manual for CTD and Trajectory data, Ifremer. <https://doi.org/10.13155/33951>, 2018.
- Wunsch, C., & Heimbach, P. (2013). Dynamically and kinematically consistent global ocean circulation and ice state estimates. In G. Siedler, S. M. Griffies, J. Gould, & J. A. Church (Eds.), *In Ocean Circulation and Climate: A 21 Century Perspective, International Geophysics* (Vol. 103, pp. 553–579). Oxford, UK: Academic Press. <https://doi.org/10.1016/B978-0-12-391851-2.00021-0>
- Yan, Y., Chassignet, E. P., Qi, Y., & Dewar, W. K. (2013). Freshening of subsurface waters in the Northwest Pacific Subtropical Gyre: Observations and dynamics. *Journal of Physical Oceanography*, 43(12), 2733–2751. <https://doi.org/10.1175/jpo-d-13-03.1>
- Zhang, L., & Qu, T. (2014). Low-frequency variability of South Pacific Tropical Water from Argo. *Geophysical Research Letters*, 41, 2441–2446. <https://doi.org/10.1002/2014GL059490>
- Zhang, R.-H., Gao, C., Kang, X., Zhi, H., Wang, Z., & Feng, L. (2015). ENSO modulations due to interannual variability of freshwater forcing and ocean biology induced heating in the tropical Pacific. *Scientific Reports*, 5, 18506. <https://doi.org/10.1038/srep18506>
- Zheng, F., Wang, H., & Wan, L. (2015). Effects of interannual salinity variability on the dynamic height in the western equatorial Pacific as diagnosed by Argo. *Acta Oceanologica Sinica*, 34(5), 22–28. <https://doi.org/10.1007/s13131-015-0663-2>